Acta Astronautica 245 (2026) 632–642

Contents lists available at ScienceDirect

Acta Astronautica

journal homepage: www.elsevier.com/locate/actaastro

Impulsive manoeuvre reconstruction from public orbit data

Yeerang Lim, Camilla Colombo *

Department of Aerospace Science and Technology, Politecnico di Milano, Via La Masa 34, 20156, Milano, Italy

ARTICLE INFO

Keywords:
Space situational awareness
Impulsive manoeuvre reconstruction
Gauss' planetary equations
Least square estimation

ABSTRACT

As the importance of space situational awareness grows along the rapid increase of artificial objects in the orbital regimes, understanding behaviours of those objects can provide useful information that is not always public. To this end, a novel formulation to identify and characterise an impulsive manoeuvre from historical data is presented, based on the least-square optimisation which is widely used for orbit determination. The Gauss' Planetary Equations are aggregated together with the Keplerian element formulation, which leads to a linear relationship between an impulsive manoeuvre and orbit elements difference. An epoch of the manoeuvre can be identified by searching the true anomaly which minimises the difference between the observations and the least-square solution. The proposed approach is validated against real orbit data from the Sentinel-3A spacecraft.

1. Introduction

TRACKING and identifying unknown events in the space environment from historical data plays a significant role for space traffic coordination, especially as the population of artificial objects in orbital regimes grows drastically and as manoeuvre histories are often not communally published. Understanding data thereof often provides useful information that is not necessarily shared, from which objects of the population are active and manoeuvrable, to which behaviours can be anticipated and considered in the decision-making. Manoeuvre detection and characterisation have been an essential element in space situational awareness within this context [1–7]. Such estimation is possible by aggregating the orbit dynamics together with observation data. If there are significant changes monitored in a spacecraft trajectory which cannot be explained solely by orbit propagation, thrusting manoeuvres or an event which has the equivalent impact can be presumed, a collision for example.

Previous works focused mainly on event detection part from existing data based on statistical techniques [1–3]. Two Line Elements (TLE) data is often utilized as database owing to its public accessibility and its updates on a regular basis. Patera developed the moving window technique, which serves to remove smaller variations due to perturbations or measurement noises while responding to slower secular variations [1]. The approach was applied to detect various events, i.e. collisions, manoeuvres, even space weather events due to the increased solar activity. Focusing on the manoeuvre detection, orbital boost manoeuvres were detected from changes in the vehicle's energy. Similar to Patera, Kelecy et al. also proposed an approach to detect abrupt changes in orbital parameters by identifying aberrantly large differences [2]. Data difference detection from adjacent segments of the smoothed data between sliding intervals is proposed. A polynomial fit is calculated both for the trailing segments and the leading segments, and the extrapolated difference between the two polynomials is examined. Both fine controls and orbit control manoeuvres were detected from the orbital energy and inclination plots. Lemmens and Krag proposed the TLE Consistency Check (TCC) as well as the TLE Time Series Analysis (TTSA) [3]. The TCC approach is based on consistency checking between consecutive TLEs of an object and the comparison of this consistency with a reference population, while the TTSA falls into the category of applying outlier statistics on the time series.

There are relatively fewer literature sources addressing manoeuvre reconstruction. While calculating a delta-v magnitude directly from a jump in the semi-major axis or in the inclination history is commonly used, there are two studies estimating manoeuvre vectors and their epochs from observation data [4,5]. Both Pastor et al. [4] and Porcelli et al. [5] used raw measurements for maintaining catalogues of the Resident Space Objects (RSOs) as it helps to avoid sets of duplicated

* Corresponding author.
E-mail addresses: yeerang.lim@polimi.it (Y. Lim), camilla.colombo@polim.it (C. Colombo).

https://doi.org/10.1016/j.actaastro.2026.02.030
Received 7 October 2025; Received in revised form 10 February 2026; Accepted 15 February 2026
Available online 16 February 2026

Nomenclature

a	= semi-major axis (km)
e =	eccentricity
f =	true anomaly (rad)
i =	inclination (rad)
M =	mean anomaly (rad)
n =	mean motion (rad/sec)
Ω =	right ascension of the ascending node (rad)
ω =	argument of perigee (rad)
λ =	mean argument of latitude (rad)
θ =	argument of latitude (rad)

objects and track correlation issues. Pastor et al. applied the least square estimation to optical observations [4]. Comparable to the conventional Orbit Determination (OD), it provides manoeuvre characteristics which associate the priori and the posteriori orbits the finest. Two formulations were proposed for a single burn and a double burns case, namely track-to-orbit and orbit-to-orbit. Then Porcelli et al. extended the similar approach to the track-to-orbit case with radar observations [5], which is typical in the LEO regime. Another noticeable category is to solve an unknown manoeuvre as a part of the OD problem [6,7]. Zhou et al. [6] derives the linear relationship between state variables and an initial condition, together with an unknown manoeuvre and its time by using the State Transition Tensor (STT). Another relationship between the state variables and measurements are approximated using the second-order Taylor series. The entire OD problem is solved in an iterative framework with the first guess of the initial orbit and the manoeuvre. Ren et al. [7] models state deviations caused by an unknown impulsive manoeuvre as state noises, and check the Noise Matching Factor (NMF) as an indicator of manoeuvring, followed by the iterative Kalman Filter with the State Noise Compensation (SNC). The performance verified using angle-with-range and and-only measurements shows the approach works under the highly nonlinear dynamics.

We introduce here a new formulation for identification and characterisation of an impulsive manoeuvre from historical data based on the least-square optimisation. The Keplerian orbit elements are chosen to exploit their benefits compared to the Cartesian coordinates. They provide the shape and the orientation of an orbit instantaneously and most of the elements vary slowly over time apart of the fast angular variable. While the past literature mainly focuses on the event detection from the trajectory deviation, we attempt to educe the most information possible about the manoeuvre from the orbit catalogues. The Gauss' Planetary Equations in literature are aggregated together with the Keplerian element formulation for the manoeuvre identification, which not only leads to linear relationships between an impulse and the orbit elements difference, but also can be propagated with the State Transition Matrix (STM) at the same time. This formulation can be transformed into a linear least square problem as a function of the true anomaly of the manoeuvring point without loss of generality. A manoeuvre can be identified by searching the optimal true anomaly i.e. the epoch of the manoeuvre, which minimises the residual between the orbit measurement and the propagation of the least-square solution delta-v to the epoch of measurement. While the first validation is available in Ref. [8], a feasibility of the proposed approach is validated again thoroughly with simulations as well as real orbits, in forms of the sp3 (Standard Product 3, also known as precise ephemeris) and the TLE data [9,10] of the Sentinel-3A satellite.

2. Manoeuvre reconstruction via gauss' Planetary Equation

When a discontinuous change in a spacecraft trajectory induced by an impulsive manoeuvre emerges, a linear relationship between a manoeuvre vector $\delta\mathbf{v} = [\delta v_T \quad \delta v_N \quad \delta v_H]^T$ in the tangential-normal-out-of-plane (TNH) frame and consequential changes in the classical orbit elements $\delta\boldsymbol{\alpha} = [\delta a \quad \delta e \quad \delta i \quad \delta\Omega \quad \delta\omega \quad \delta M]^T$ is given as the Gauss' Planetary Equation as a function of the true anomaly f [11],

$$\mathbf{G}_v(f) = \begin{bmatrix} \frac{2a^2v}{\mu} & 0 & 0 \\ \frac{2(e+\cos f)}{v} & -\frac{r}{av}\sin f & 0 \\ 0 & 0 & \frac{r\cos\theta}{h} \\ 0 & 0 & \frac{r\sin\theta}{h\sin i} \\ \frac{2\sin f}{ev} & \frac{2e+(r/a)\cos f}{ev} & -\frac{r\sin\theta\cos i}{h\sin i} \\ -\frac{b}{eav}2\left(1+\frac{e^{2r}}{p}\right)\sin f & -\frac{b}{eav}\frac{r}{a}\cos f & 0 \end{bmatrix} \tag{1}$$

where $b = a\sqrt{1-e^2}$ is the semi-minor axis of the orbit, $p = a(1-e^2)$ is the semilatus rectum, h is the norm of the angular momentum, v is the velocity magnitude, and r is the radial distance. Assume that two states in the Keplerian elements $\boldsymbol{\alpha}_0$ and $\boldsymbol{\alpha}_f$ are available at the epoch t_0 and t_f respectively, which makes $\boldsymbol{\alpha}_0 = \boldsymbol{\alpha}(t_0)$ and $\boldsymbol{\alpha}_f = \boldsymbol{\alpha}(t_f)$, and the difference between the two states cannot be explained by propagation. An impulsive manoeuvre within $[t_0, t_f]$ is presumable, with its epoch $t = t_f - \Delta t$ to be solved.

It is inherently a Two-Point Boundary Value Problem (TPBVP) with an unknown Δt as shown in Fig. 1. If a linear propagation of the error states $\delta\boldsymbol{\alpha}$ is available in the form of the STM $\mathbf{G}_M$, the problem can be written as Eq. (2).

$$\delta\boldsymbol{\alpha}(t_f) = \mathbf{G}_M\left(\Delta t, \boldsymbol{\alpha}(t)|_{\boldsymbol{\alpha}_f}\right)\mathbf{G}_v\left(t, \boldsymbol{\alpha}(t)|_{\boldsymbol{\alpha}_0}\right)\delta\mathbf{v} = \mathbf{G}(\Delta t)\delta\mathbf{v} \tag{2}$$

It is worth noting that the different orbit elements should be used to calculate the $\mathbf{G}_v$ and the $\mathbf{G}_M$ respectively, as there are two measurements which supposedly have a discontinuous change in the middle. And assuming $\delta\boldsymbol{\alpha} \ll \boldsymbol{\alpha}$, a straightforward way to derive the $\mathbf{G}_M$ is to take the first-order approximation of the Keplerian motion.

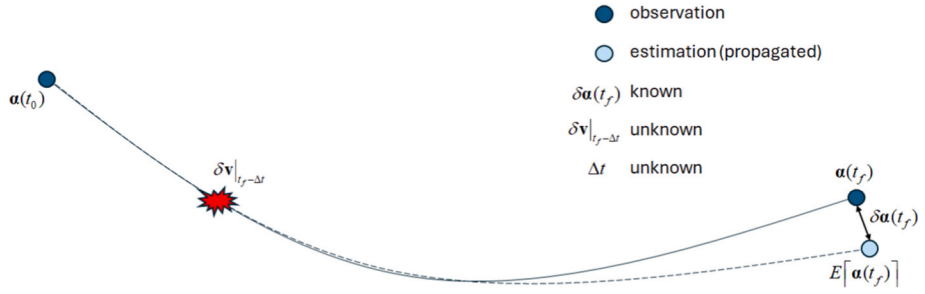

Fig. 1. Schematic problem definition of the manoeuvre reconstruction [8].

Table 1
Test case (1) – initial and final orbits, the Keplerian orbit.

Initial orbit @ modified Julian date 21545					
X (km)	Y (km)	Z (km)	V_X (km/sec)	V_Y (km/sec)	V_Z (km/sec)
7100	0	1300	0	7.35	1
Final orbit @ modified Julian date 21545.486					
X (km)	Y (km)	Z (km)	V_X (km/sec)	V_Y (km/sec)	V_Z (km/sec)
6118.054	−3598.886	629.441	3.757	6.322	1.551

Table 2
Test case (1) – $\delta\mathbf{v}$ to be solved.

t_0 (modified Julian date)	21545
t_f (modified Julian date)	21545.486
Δt (sec)	30000
$t_{\delta v}$	$t_0 + 12000$ s
$\delta\mathbf{v}$ (TNH)	$[2.0 \quad 0 \quad 3.0]^T$ (m/sec)

$$\mathbf{G}_M\left(\Delta t, \boldsymbol{\alpha}(t)|_{\alpha_f}\right) = \begin{bmatrix} 1 & \mathbf{0}_{1\times4} & 0 \\ \mathbf{0}_{4\times1} & \mathbf{I}_{4\times4} & 0 \\ -\frac{3}{2}n\Delta t & \mathbf{0}_{1\times4} & 1 \end{bmatrix} \tag{3}$$

Since the matrix $\mathbf{G}(\Delta t)$ is 6x3, solving the $\delta\mathbf{v}$ is an over-determined problem, meaning that there is no solution in general and therefore the problem can be solved only in a statistical way, i.e. regression analysis. In this respect, the problem in Eq. (2) can be converted to an optimal Δt searching in the $[t_0, t_f)$, which minimises

$$\left\|\delta\boldsymbol{\alpha}(t_f) - \mathbf{G}(\Delta t)\delta\mathbf{v}_{LSQ}\right\| \tag{4}$$

By assuming a fixed Δt, the least-square solution is available as below [8].

$$\delta\mathbf{v}_{LSQ} = \left(\mathbf{G}^T\mathbf{G}\right)^{-1}\mathbf{G}^T\delta\boldsymbol{\alpha} \tag{5}$$

When there is no perturbation or measurement noise present, Eq. (4) becomes zero with the correct Δt.

It is worth noting that the formulation is based on the single impulse assumption. If there are multiple burns between the initial and the final points and only the boundary conditions are given, there will be transfer orbits which are not fixed, which would make the formulation more of an optimal control problem and the proposed approach not applicable. Moreover, the Δt search will become multi-dimensional. The same applies to the problem with a low thruster, only an optimal manoeuvre profile to minimize a cost function can be solved [12].

The problem defined in Eq. (4) and Eq. (5) is validated with numerical simulations. An initial orbit in Table 1 is propagated with NASA's GMAT [13] from 21545 MJD, with an impulsive manoeuvre described in Table 2. The EGM-96 gravity model with 0 degree and 0 order is used first, i.e. the Keplerian orbit propagation, hence the Earth oblateness or the atmospheric drag is not included in the propagation.

Fig. 2 shows the error magnitude with the least square solution in Eq. (4) for each Δt candidates. The red plot in the same figure shows the $\delta\mathbf{v}$ magnitude of each least square solution. As shown in Fig. 2 and also as summarised in Table 3, the Δt with the minimum error matches with the true value in Table 2, also the manoeuvre vector is estimated quite well.

The same condition is simulated again, repeated with the EGM-96 gravity model with the 2 degree and the 2 order this time, which adds the Earth J_2 perturbation during the propagation as in Table 4.

The result is summarised in Table 5 The $\delta\mathbf{v}$ estimation is significantly degraded compared to the previous result by assuming the Keplerian motion in the STM, especially for the normal direction δv_N. The epoch of the manoeuvre is not estimated correctly as well.

This means that the linearised propagation does not reflect the actual behaviour of the trajectory. To overcome this issue, the number of states

Table 3
Test case (1) – manoeuvre estimation result, the Keplerian orbit.

$\delta\mathbf{v}_{LSQ}$	$[2.001 \quad -0.045 \quad 2.996]^T$ (m/sec)
$\|\|\delta\mathbf{v}_{LSQ} - \delta\mathbf{v}\|\|/\|\|\delta\mathbf{v}\|\|$	1.25 %
Δt (sec)	30000

Table 4
Test case (2) – Final orbit, under the EGM 2x2.

Final orbit @ modified Julian date 21545.486					
X (km)	Y (km)	Z (km)	V_X (km/sec)	V_Y (km/sec)	V_Z (km/sec)
6429.593	−2970.266	848.574	3.096	6.688	1.435

Table 5
Test case (2) – manoeuvre estimation result, under the EGM 2x2.

$\delta\mathbf{v}_{LSQ}$	$[1.6652 \quad -2.1689 \quad 2.5145]^T$ (m/sec)
$\|\|\delta\mathbf{v}_{LSQ} - \delta\mathbf{v}\|\|/\|\|\delta\mathbf{v}\|\|$	62.34 %
Δt (sec)	35700

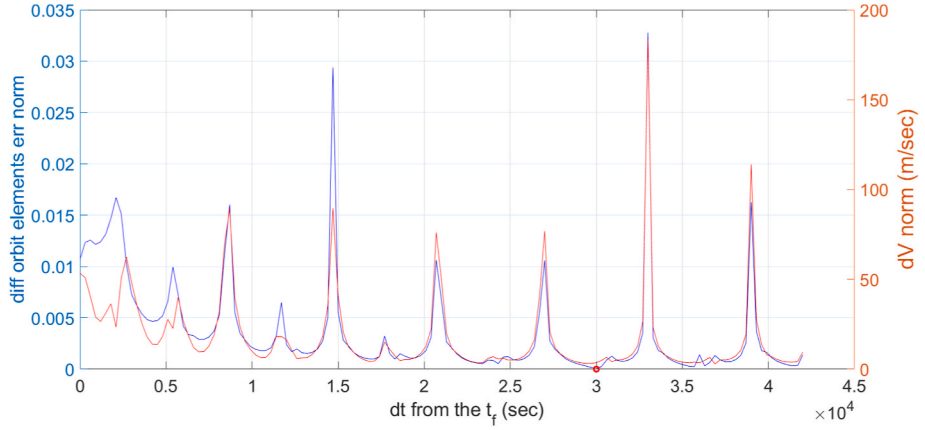

Fig. 2. Test case (1) – least square solution search, the Keplerian orbit

Table 6
Test case (2) – manoeuvre estimation result, under the EGM 2x2, the secular terms considered.

$\delta\mathbf{v}_{LSQ}$	$[2.003 \quad -0.051 \quad 2.944]^T$ (m/sec)
$\lvert\lvert\lvert\delta\mathbf{v}_{LSQ} - \delta\mathbf{v}\rvert\rvert\rvert / \lVert\delta\mathbf{v}\rVert$	2.12 %
Δt (sec)	30000

is reduced from 6 to 5 first by replacing the ω and the M by the argument of latitude λ,

$$\mathbf{G}_{\nu}\left(t, \boldsymbol{\alpha}(t)|_{\boldsymbol{\alpha}_0}\right) = \begin{bmatrix} \frac{2a^2\nu}{\mu} & 0 & 0 \\ \frac{2(e+\cos f)}{\nu} & -\frac{r}{a\nu}\sin f & 0 \\ 0 & 0 & \frac{r\cos\theta}{h} \\ 0 & 0 & \frac{r\sin\theta}{h\sin i} \\ \left(\frac{2\sin f}{e\nu} - \frac{b}{ea\nu}2\left(1+\frac{e^{2r}}{p}\right)\sin f\right) & \left(\frac{2e+(r/a)\cos f}{e\nu} - \frac{b}{ea\nu}\frac{r}{a}\cos f\right) & -\frac{r\sin\theta\cos i}{h\sin i} \end{bmatrix} \tag{6}$$

and the STM is updated to include the secular effect due to the Earth J_2 oblateness [14],

$$\mathbf{G}_{M}\left(\Delta t, \boldsymbol{\alpha}(t)|_{\boldsymbol{\alpha}_f}\right) = \begin{bmatrix} 1 & \mathbf{0}_{1\times3} & 0 \\ \mathbf{0}_{3\times1} & \mathbf{I}_{3\times3} & 0 \\ -\frac{3}{2}n\Delta t & \mathbf{0}_{1\times3} & 1 \end{bmatrix} + \begin{bmatrix} 0 & 0 & 0 & 0 & 0 \\ 0 & 0 & 0 & 0 & 0 \\ 0 & 0 & 0 & 0 & 0 \\ 7\kappa R & -8\kappa eGR & 2\kappa U & 1 & 0 \\ -\frac{7}{2}\kappa\eta(Q+P) & \kappa e\eta G(4Q+3P) & -\kappa(5S+3\eta S) & 0 & 0 \end{bmatrix}\Delta t \tag{7}$$

where $\eta = \sqrt{1-e^2}$, $\kappa = \frac{3}{4}\frac{J_2 R_E{}^2\sqrt{\mu}}{a^{7/2}\eta^4}$, $G = \frac{1}{\eta^2}$, $P = 3\cos^2 i - 1$, $Q = 5\cos^2 i - 1$, $R = \cos i$, $S = \sin(2i)$, $U = \sin i$. The same estimation is repeated with the updated STM, and the result is dramatically improved (see Table 6).

Another thing worth mentioning is the drag effect, especially for the Low Earth Orbit (LEO) regime. Although several variations of the STM are available in Ref. [14] to consider the differential drag in the relative states' propagation, the additional terms vanish in Eq. (5) as the Gauss' Planetary Equation does not have any states representing time derivatives of the orbit elements. Therefore, it is possible to consider the drag effect only in the $\delta\boldsymbol{\alpha}(t_f)$, namely when calculating the expected final states. The errors stay under 2 % in the same simulation when a correct ballistic coefficient is used in the propagation, while the error becomes almost 30 % when the atmospheric model is not included in the propagation. This is expected from the least-square formulation in Eq. (5), as the $\delta\nu$ is estimated using the $\delta\boldsymbol{\alpha}(t_f)$. Consequently it is required to use the realistic STM as well as the final states. From this context, the

Table 7
Comparison of the sp3 and the TLE orbit data.

	sp3	TLE
Data	List of satellite position and velocity at a certain epoch	A set of orbit elements (mean elements for SGP4 propagator) at a certain epoch
Update frequency	Every 60 s	Varies from several times a day (for LEO) to once or twice a week (low-drag orbit)
Accuracy	Range of centimetres	Range of kilometres for the initial epoch, degradation foreseen for longer propagation time
Coverage	Selected objects only	All orbiting objects bigger than a certain size

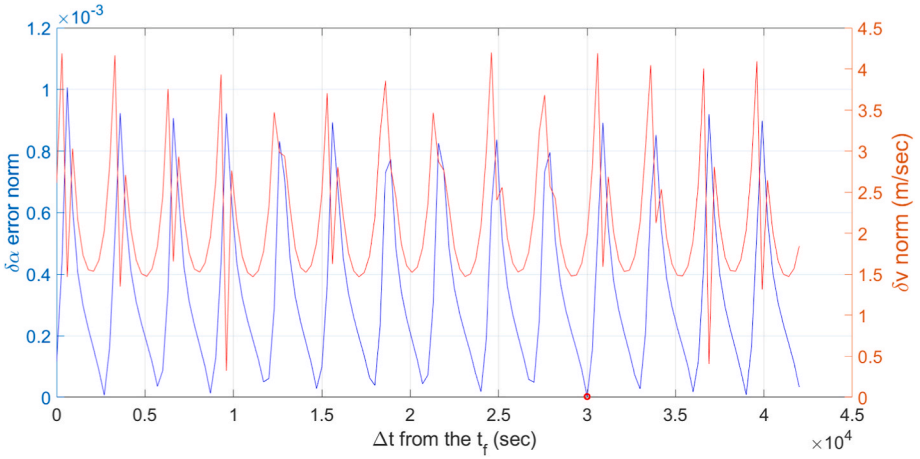

Fig. 3. Out-of-plane manoeuvre only – least square solution search

Table 8
Sentinel out-of-plane manoeuvre history.

Manoeuvre epoch	2024 March 07 11:27:19.349
$\delta\mathbf{v}$ (TNH)	$[0.0219 \quad 0.0018 \quad 2.2917]^T$ (m/sec)

same simulation holds less than 5 % error under the EGM 10x10, when the same high-fidelity gravity model is used to calculate the $\delta\boldsymbol{\alpha}(t_f)$.

There are a couple of other notes to be addressed. First, due to the linearised dynamics, the estimation will become less accurate when the window for the Δt search is too wide. Second, an orbital ambiguity in the estimation is foreseen if there is no change in the semimajor axis. An example can be an out-of-plane manoeuvre only case, which does not affect the in-plane motion. As can be observed in Fig. 3, the difference between the least-square solution and the observed $\delta\boldsymbol{\alpha}(t_f)$ is almost periodic and there is no significant different observed as in Fig. 2. In this case it is possible for the algorithm to find the correct $\delta\mathbf{v}$ with a wrong Δt at the same orbital phase. Moreover, it is also possible to estimate the $\delta\mathbf{v}$ with the opposite sign with a phase difference of $+\pi$. This point will be revisited more in detail in the following section. Lastly, the current formulation is based on the two-body motion with respect to the Earth.

3. Manoeuvre reconstruction from actual orbit data

The proposed approach is tested with two types of the actual orbit data, the sp3 and the TLE, and an actual manoeuvre log. The manoeuvre history is available for selected spacecraft by the International DORIS Service (IDS) [15]. The differences between the sp3 and the TLE data can be summarised as below in Table 7 before presenting the results for better comparison.

3.1. SP3 data

SP3 data is available for selected satellites by NASA's Crustal Dynamics Data Information System (CDDIS) [9]. We chose an out-of-plane manoeuvre of the Sentinel-3A in Table 8 first, in the order of 1 m/s. The sp3 file provides the position and the velocity in the ITRF frame every 60 s.

We assume that the manoeuvre is already detected. The search window is set for an hour, from 11:00 to 12:00, and the EGM 30x30 gravity model is used for propagating the expected orbit elements. Please note that, when an accurate reconstruction of a manoeuvre is a concern in Fig. 4, the osculating orbit elements and the mean orbit elements should be distinguished and to be used accordingly, as well as the transformation between the two.

The least square estimation result is summarised in Table 9. Even without considering the drag effect in the propagation, it provides an accurate estimate.

Table 9
Sentinel out-of-plane manoeuvre reconstruction (1).

$\delta\mathbf{v}_{LSQ}$	$[0.0324 \quad 0.0287 \quad 2.1518]^T$ (m/sec)
$\|\|\delta\mathbf{v}_{LSQ} - \delta\mathbf{v}\|\|/\|\|\delta\mathbf{v}\|\|$	6.26 %
Manoeuvre epoch	11:27

Table 10
Sentinel out-of-plane manoeuvre reconstruction (2).

$\delta\mathbf{v}_{LSQ}$	$[0.0790 \quad 0.0489 \quad 2.3139]^T$ (m/sec)
$\|\|\delta\mathbf{v}_{LSQ} - \delta\mathbf{v}\|\|/\|\|\delta\mathbf{v}\|\|$	3.84 %
Manoeuvre epoch	02:36

For the same manoeuvre reconstruction, the search window is extended to 24 h, from 00:00 March 07 to 00:00 March 08. While the $\delta\mathbf{v}$ estimation is still working fine as shown in Table 10, the Δt estimation differs more than 8 h from the actual epoch.

As addressed in the previous section, we suspect that this is due to the periodic evolution of the trajectory as shown in Fig. 5 when the out-of-plane manoeuvre is dominant. Therefore, it is recommended to narrow down the search window when a manoeuvre epoch can be roughly estimated.

Then an in-plane manoeuvre in Table 11 is reconstructed, which is the first part of an orbit raising manoeuvres with two impulses.

Here we examine that the $\delta\mathbf{v}$ estimation is not accurate, especially in the normal direction. Another interesting point is that the tangential impulse is well reconstructed at the same time. This is caused by the large uncertainty in the along-track coordinate. The tangential impulse δv_T can be estimated mostly from the semi-major axis difference, as it is only affected by a tangential manoeuvre.

Although it sounds probable, the exact ballistic coefficient or the attitude is not available to calculate the accurate $\delta\boldsymbol{\alpha}(t_f)$. So we decided to fully utilise the benefit of the sp3 data type, which records the coordinates every minute. Revisiting Eq. (2), the Δt increases reservedly from the t_f to the t_n. Instead of propagating the coordinates from the t_n to the t_f with the single STM, STMs from an $\boldsymbol{\alpha}(t_i)$ to an $\boldsymbol{\alpha}(t_{i+1})$ for every $t_i \in [t_n, t_f)$ are calculated and multiplied to reach t_f as illustrated in Fig. 6.

Using this approach, the propagation time can be maintained the same as the frequency of the measurements, and the orbit elements difference caused by the drag will be smaller as each measurement already contains its effect. Indeed, comparing Table 13 with the previous Table 12, the order of the δv_N error decreases from 1e-1 to 1e-2. Fig. 7 shows the error magnitude and the corresponding $\delta\mathbf{v}$ over time.

Lastly, the same approach is applied to a smaller in-plane manoeuvre

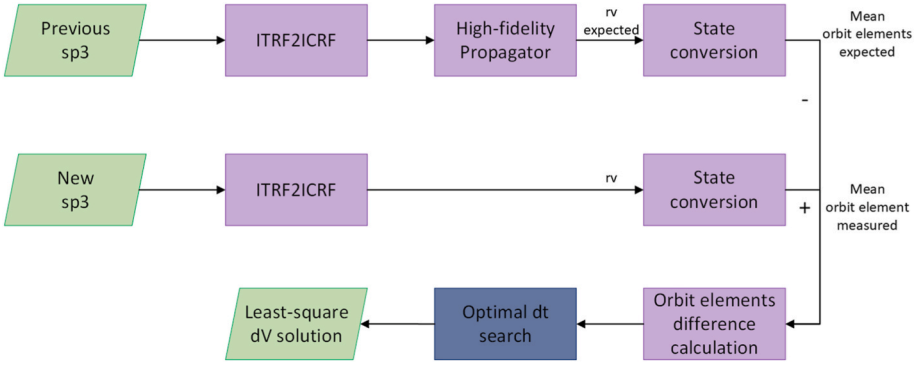

Fig. 4. Manoeuvre reconstruction process from the sp3 data

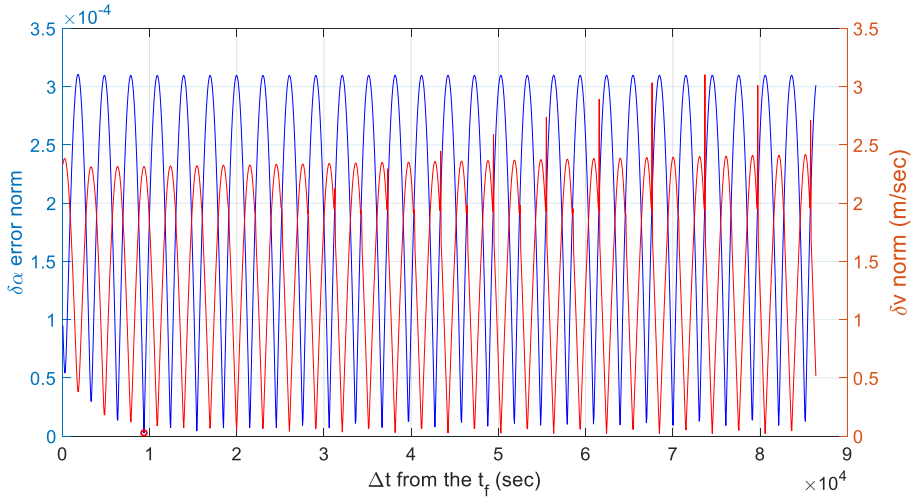

Fig. 5. Sentinel out-of-plane manoeuvre – least square solution search

Table 11
Sentinel in-plane manoeuvre history (1).

Manoeuvre epoch	2022 January 07 00:10:37.000
$\delta\mathbf{v}$ (TNH)	$[0.1225 \quad 0.0003 \quad 0.0035]^T$ (m/sec)

in Table 14. The search window is an hour, from 09:30 to 10:30 March 14.

While the performance of δv_T and the manoeuvre epoch remains similar to Table 13, the δv_N of 1e-2 order is not negligible due to the small manoeuvre magnitude (see Table 15 and Fig. 8). We suspect this order of the δv_N error is from the accuracy of $\delta\boldsymbol{\alpha}(t_f)$ calculation, which includes errors both in the measurements and in the propagation.

Table 12
Sentinel in-plane manoeuvre reconstruction (1-1).

$\delta\mathbf{v}_{LSQ}$	$[0.1237 \quad 0.1236 \quad 0.0060]^T$ (m/sec)
$\lvert\lvert\delta\mathbf{v}_{LSQ} - \delta\mathbf{v}\rvert\rvert / \lvert\lvert\delta\mathbf{v}\rvert\rvert$	101.2 %
$\left\lvert\left\lvert\delta v_{T,LSQ} - \delta v_T\right\rvert\right\rvert / \lvert\lvert\delta v_T\rvert\rvert$	1.22 %
Manoeuvre epoch	00:00

3.2. TLE data

Then we applied the same approach to the TLE data [10], which is the most available. To apply the approach to the actual TLE history, the outlier removal is applied [16]. We do not address the outlier filtering in detail here; it can be summarised in six steps as follow.

i. Filter out the TLEs that were published but subsequently corrected.
ii. Filter large time gaps between the TLEs because they hinder proper verification of the TLE consistency.
iii. Identify any single TLE with an inconsistent mean motion, as well as the entire sequences thereof, using the sliding window approach.
iv. Filter out the TLEs outlying in the eccentricity.
v. Filter out the TLEs outlying in the inclination.
vi. Filter out the TLEs with negative B* values.

Once the filtered TLEs are obtained, the edges of the discontinuous jumps in the elements are selected as the initial and the final point of the problem. Please note that we do not consider the manoeuvre detection here, so for now a peak in the TLE history is manually picked up after the

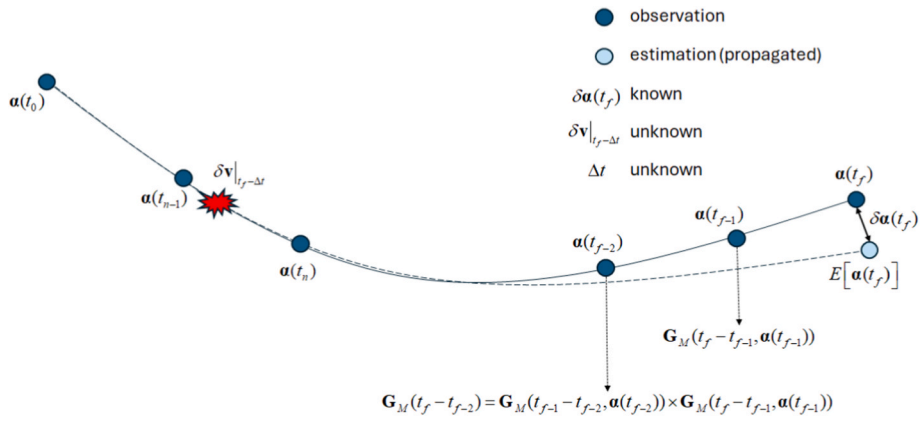

Fig. 6. Manoeuvre reconstruction with the recursive STM calculation

$$\mathbf{G}_M(t_f - t_n) = \prod_{i=n}^{f-1} \mathbf{G}_M(t_{i+1} - t_i, \boldsymbol{\alpha}(t_i)) \tag{7a}$$

outliers are filtered. Fig. 9 shows the simulation process. When a manoeuvre is detected from the TLE, the mean orbit elements are compared with the propagated ones from the previous TLE. Once the error mean orbit elements are calculated, the optimal Δt and the corresponding least square solution search are started within the given time window.

One thing worth mentioning is that the effect of a manoeuvre is lagged in the TLE data, although the manoeuvre itself lasts a few thousand seconds at the maximum. The delay is visible in Fig. 10, which causes two negative effects. First, it makes the Cartesian coordinates from the SGP4 propagator less accurate. It is known that the TLE accuracy is around 1 km at its initial epoch, and grows 1 to 2 km per day. If the full effect from the manoeuvre appears after 10 days, the propagation adds 10 to 20 km errors in the $\delta\boldsymbol{\alpha}(t_f)$, which might overshadow the manoeuvre effect considering the magnitude of the routine maintenance. Second, it makes the linearised STM less accurate.

On that note, we applied the same approach to the TLE data from the Sentinel-3A between year 2023 to 2025. The estimation of the manoeuvre epoch is not presented here. Again, the TLE starts increasing after a manoeuvre takes place, which makes the epoch estimation less meaningful. First, we examine an out-of-plane manoeuvre in Table 16. It is obvious that the out-of-plane components are estimated in the same order, however often with the opposite sign. This is expected from the periodic evolution of the orbit, as already described in the previous section. Therefore, only the magnitude of the out-of-plane impulses are compared to the reference values.

Then the in-plane manoeuvres in Table 17 are examined. It should be noted that the in-plane manoeuvres with 1e-1 m/s order as from the Sentinel-3A in Table 11 cannot be considered with the TLEs, as larger orbit raising manoeuvres often conducted in a pair (as the Homann transfer). It is possible to isolate a single manoeuvre in the sp3 data, but in the TLE there will be the second manoeuvre already before the TLE reflects the full effect of the first impulse. Consequently the δv_T magnitudes are in the order of 1e-2 m/s, which makes the reconstruction more challenging considering the nominal TLE accuracy.

One interesting point is that the only epoch where the estimated out-of-plane manoeuvre is in 1 m/s level, is where an actual out-of-plane manoeuvre took place. This provides a clue of the sensitivity of the proposed algorithm with the TLEs. It is noticeable that, while the manoeuvres are in the tangential direction, the estimation provide a large δv_N in the most cases. We suspect the poor accuracy in the argument of latitude leads to the large δv_N to make the error residuals smaller. Also, the order of the error for the out-of-plane manoeuvres are relatively higher than the error in the tangential manoeuvres in Table 16. This will be discussed more in detail in the following section.

Table 13
Sentinel in-plane manoeuvre reconstruction (1-2).

$\delta\mathbf{v}_{LSQ}$	$[0.1233 \quad -0.0147 \quad 0.0072]^T$ (m/sec)
$\lvert\lvert\lvert\delta\mathbf{v}_{LSQ} - \delta\mathbf{v}\rvert\rvert\rvert / \lvert\lvert\delta\mathbf{v}\rvert\rvert$	12.17 %
$\left\lvert\left\lvert\left\lvert\delta v_{T\_LSQ} - \delta v_T\right\rvert\right\rvert\right\rvert / \lvert\lvert\delta v_T\rvert\rvert$	0.65 %
Manoeuvre epoch	00:12

4. Sensitivity analysis

A sensitivity analysis is conducted under two scenarios, (1) an inclination change and (2) an energy raising. It is tricky to perform a single, unified analysis, as the performance of the manoeuvre estimation depends not just on the perturbation magnitude but also on the magnitude and the direction of the reference manoeuvre. Hence the case scenarios were dissected into two cases, (1) when there is a 1.0 m/s out-of-plane manoeuvre happened and (2) a 1.0 m/s along-track manoeuvre happened. Then standard position errors up to 100 m sigma-value in the transverse/along-track/orbit-normal direction added for each case. For each sigma-value, a Monte Carlo study is performed with 50 simulations. Figs. 11–13 show the $\delta\mathbf{v}$ estimation errors in the tangential (blue), the normal (black), and the out-of-plane (magenta) direction respectively, with respect to the Cartesian coordinates error in each axis. The left plots show the sensitivity analysis for the out-of-plane manoeuvre estimation, while the right plots show the same analysis for the along-track manoeuvre estimation.

It is quite clear that the estimation of the out-of-plane manoeuvres is more robust under the position error, comparing the axes scale between them. We suspect a couple of causes. First, changing an orbit plane costs more than raising an altitude, namely the out-of-plane estimation is less sensitive to the same level of noise. Second, an out-of-plane manoeuvre is less coupled with the in-plane motion. It can be completely decoupled if only an inclination change is considered, hence the orbit-normal estimation is not affected by the in-plane noises.

Table 14
Sentinel in-plane manoeuvre history (2).

Manoeuvre epoch	2023 March 14 09:55:37.000
$\delta\mathbf{v}$ (TNH)	$[0.0260 \quad 0.0003 \quad 0.0009]^T$ (m/sec)

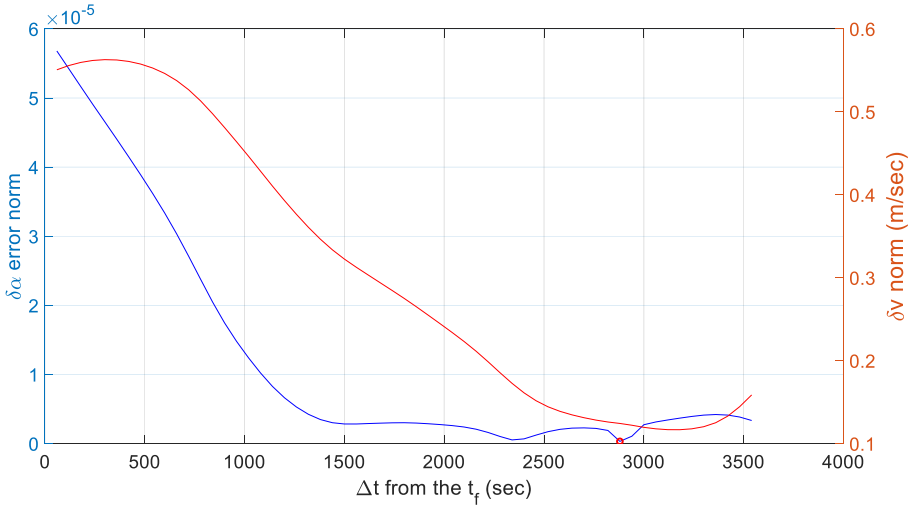

Fig. 7. Sentinel in-plane manoeuvre – least square solution search (1-2)

Table 15
Sentinel in-plane manoeuvre reconstruction (2).

$\delta\mathbf{v}_{LSQ}$	$[0.0262 \quad 0.0316 \quad -0.0008]^T$ (m/sec)
$\|\|\|\delta\mathbf{v}_{LSQ} - \delta\mathbf{v}\|\|\| / \|\|\delta\mathbf{v}\|\|$	120.6 %
$\left\|\left\|\left\|\delta v_{T,LSQ} - \delta v_T\right\|\right\|\right\| / \|\|\delta v_T\|\|$	0.77 %
Manoeuvre epoch	09:46

Moreover, the estimation in the transverse direction often contains the largest error compared to the other two axes, which can be explained from the Gauss' Planetary Equation in Eq. (1). As the semi-major axis can vary only by the along-track manoeuvre, and so is the relative inclination only by the orbit-normal manoeuvre, the algorithm is prone to make amends for the residuals by estimating (or adding) a transverse manoeuvre. Unless both the measurement and the propagation have high precisions, it is recommended to jettison the in-track estimation.

One possible way to overcome the sensitivity issue is to reduce the dimension of the problem, especially as it is envisaged that routine orbit maintenances are often done separately for an orbit raising and an orbital plane change. If one kind of maintenance is observed in the data, it is possible to extract a single axis in Eq. (1) and estimate a 1-dimensional solution. If it is presumable that the unknown manoeuvre is a routine one, it is also reasonable to assume an along-track only manoeuvre and to neglect a transverse axis. Of course, this approach is not valid for an unexpected event such as a collision or an explosion, it would not be possible to assume the direction of an such impact. Then it is necessary to have both the high-fidelity propagator, as well as the precise measurements.

5. Conclusion

A new, novel approach to characterise an unknown impulsive manoeuvre is introduced, in a form of the least-square estimation with the reverse Gauss' Planetary Equations. The proposed method is verified through the simulations with the high-fidelity propagator, followed by the application to the actual orbit data, the sp3 and the TLE.

A couple of remarks can be made, mainly on utilizing the TLE data and the sensitivity analysis of the method. First, despite the TLE accuracy and the large search window up to more than 10 days, it was possible to reconstruct a manoeuvre with the reasonable accuracies, especially for the inclination changes. It is noticeable that an out-of-plane manoeuvre is less sensitive to the observation errors. Second, the estimation is highly dependent to both data accuracy and propagation, meaning the observation should be accurate enough (imagine orbit determination), while the propagator should also consider the dominant perturbation. It is because a manoeuvre is reconstructed directly from the difference between an orbit data and the propagation. Third, due to the nature of the TLE from the batch process, the full effect of a manoeuvre may appear days after from the actual epoch, which adds delays in the estimation. Consequently it is not worthwhile to estimate

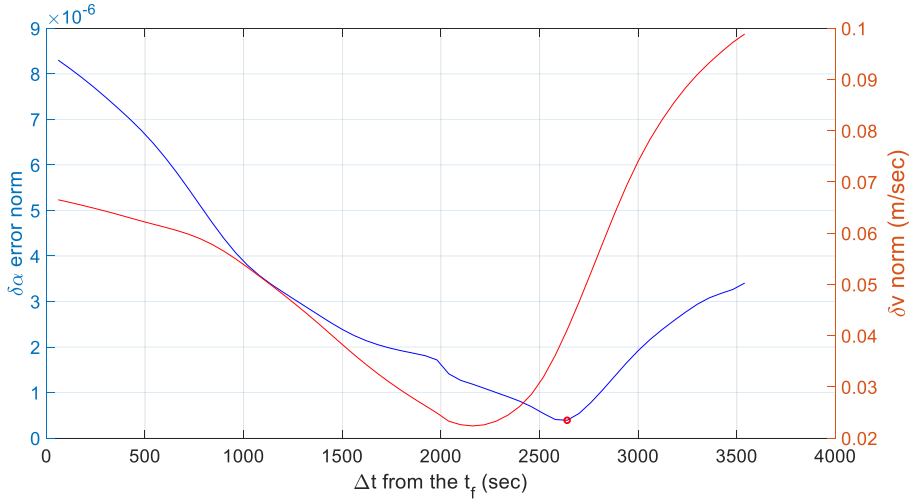

Fig. 8. Sentinel in-plane manoeuvre – least square solution search (2)

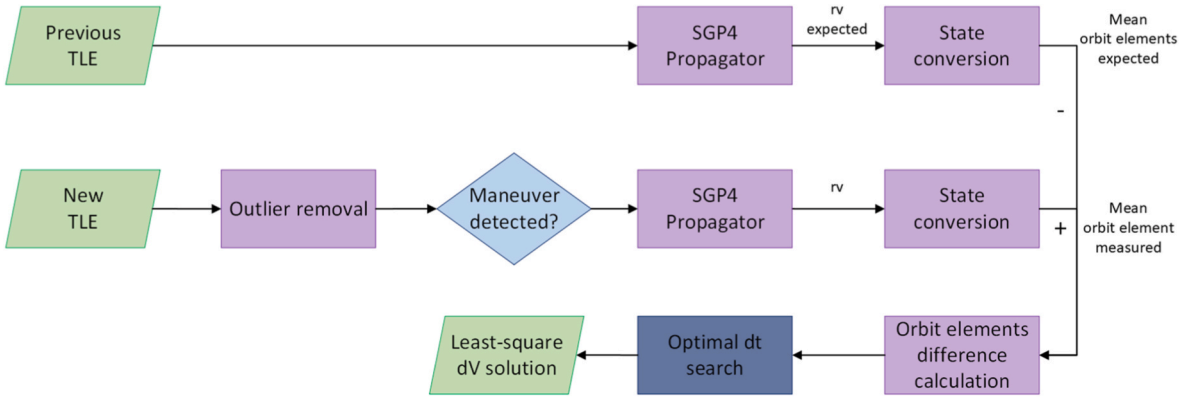

Fig. 9. Manoeuvre reconstruction process from the TLE data [8].

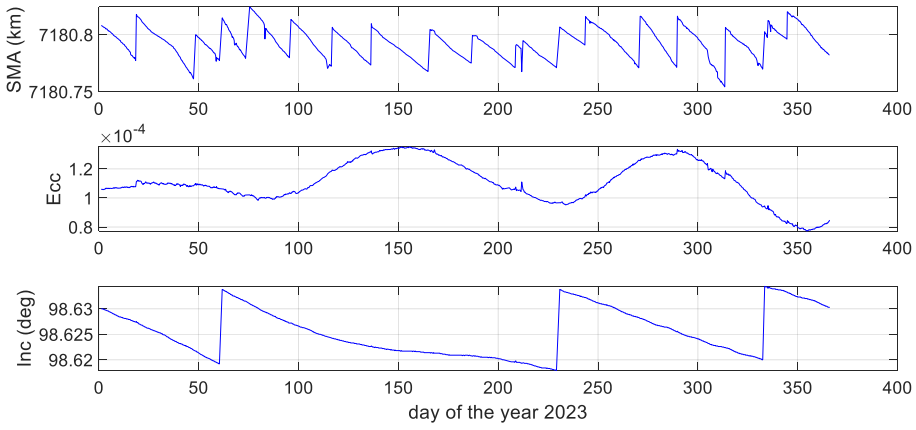

Fig. 10. Sentinel-3A TLE history after outlier removal, year 2023

Table 16
Sentinel-3A out-of-plane manoeuvre estimation, happened between 2023 and 2025.

Epoch	23060	23229	23332	24066	24246	24354	25072	25247
$\delta\mathbf{v}$ happened (m/sec, TNH)	0.0210	0.0197	0.0187	0.0219	0.0231	0.0224	0.0236	0.0253
	0.0017	0.0020	0.0012	0.0018	0.0027	0.0020	0.0014	0.0016
	2.0078	2.2422	2.0886	2.2917	2.2057	2.2043	2.2060	2.0368
$\delta\mathbf{v}$ estimated (m/sec, TNH)	0.0261	0.0204	0.0240	0.0193	0.0288	0.0226	0.0267	0.0303
	0.0134	0.0463	−0.0402	0.0054	0.0411	−0.0046	0.0094	0.0356
	−1.9116	2.1103	−1.9745	−2.1183	2.0722	2.0850	2.0691	−1.9281
$\lvert\lVert\delta\widehat{\mathbf{v}}_h\rVert - \lVert\delta\mathbf{v}_h\rVert\rvert / \lVert\delta\mathbf{v}_h\rVert$	4.79 %	5.88 %	5.46 %	7.57 %	6.05 %	5.41 %	6.21 %	5.34 %

Table 17
Sentinel-3A in-plane manoeuvre estimation, happened in 2023.

Epoch	23018	23047	23060	23073	23095	23116	23136	23165	23186
$\delta\mathbf{v}$ happened (m/sec, TNH)	0.0212	0.0212	0.0210	0.0260	0.0181	0.0178	0.0176	0.0197	0.0133
	0.0005	−0.0001	0.0017	0.0003	0.0004	0.0005	0.0004	0.0002	0.0004
	−0.0006	0.0001	2.0077	0.0009	0.0006	0.0002	0.0004	0.0001	0.0008
$\delta\mathbf{v}$ estimated (m/sec, TNH)	0.0304	0.0239	0.0261	0.0306	0.0180	0.0197	0.0177	0.0200	0.0118
	0.0354	0.1973	0.0134	0.3048	−0.0337	−0.3839	−0.0185	−0.4076	0.1590
	0.0278	0.0560	−1.9116	−0.1072	0.0684	−0.0209	0.0250	0.0471	0.0503
$\lvert\lVert\delta\widehat{\mathbf{v}}_T\rVert - \lVert\delta\mathbf{v}_T\rVert\rvert / \lVert\delta\mathbf{v}_T\rVert$	43.40 %	12.74 %	24.29 %	17.70 %	0.55 %	10.67 %	0.57 %	1.52 %	11.28 %

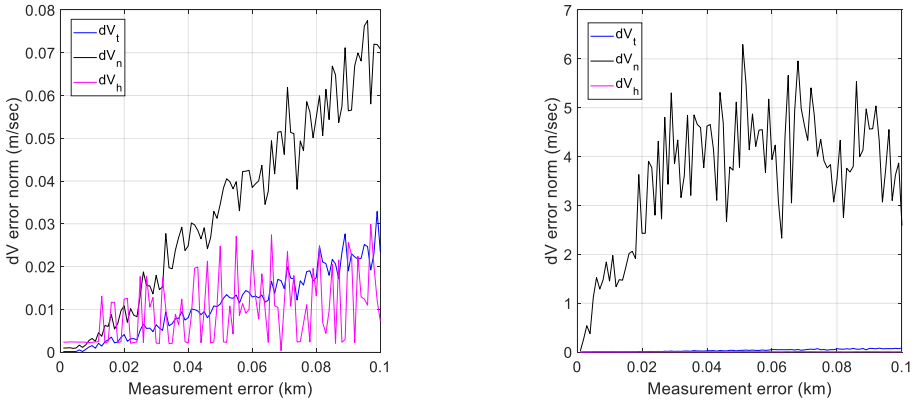

Fig. 11. Error sensitivity analysis, normal direction, out-of-plane (left) and in-plane (right) case

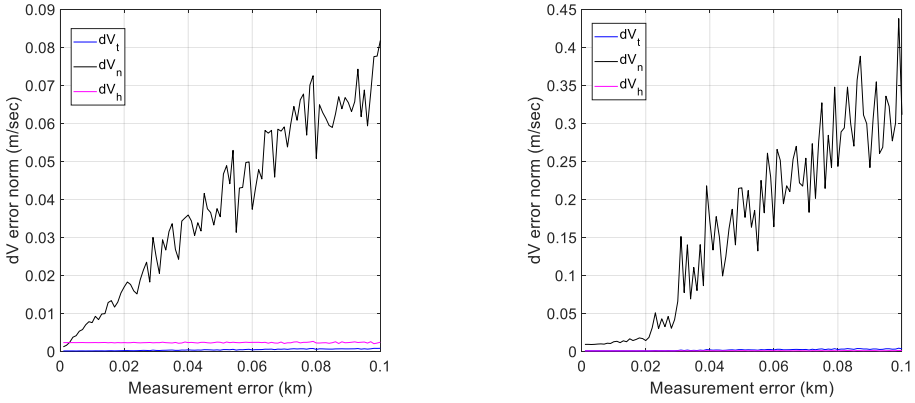

Fig. 12. Error sensitivity analysis, tangential direction, out-of-plane (left) and in-plane (right) case

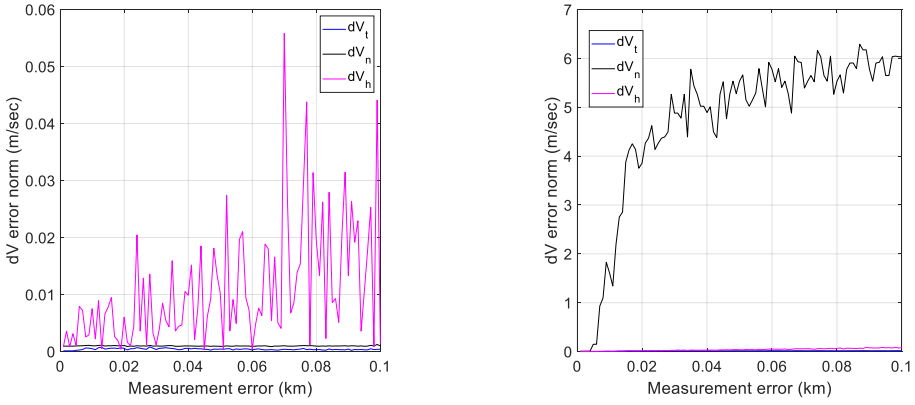

Fig. 13. Error sensitivity analysis, out-of-plane direction, out-of-plane (left) and in-plane (right) case

the manoeuvre epoch from the TLE data. Last but not least, considering its sensitivity, it is not recommended to use the in-track manoeuvre estimation, when the level of data accuracy is low and the propagation time is long. It provides a more reliable estimation when the data reflects the manoeuvres instantly, in sp3 for instance.

In case of a cooperative spacecraft, one can think of combining the sp3 (or the equivalent high precision data) and the TLE. A manoeuvre can be detected directly from the mean orbit elements plot from the TLEs. Once a manoeuvre is detected, the manoeuvre reconstruction from the sp3 data can be activated. The search window can be narrowed down to the first part of the non-natural change in the orbit. Following this way the computational load on the detection part can be saved. If the TLE is the only available data, on the other hand, we recommend considering the level of uncertainty in the different orbit elements calculation, especially for the along-track component. The uncertainty of the calculation could be used as a threshold, if the along-track coordinate is within the uncertainty, then it can be considered to discard the estimated normal impulse.

CRediT authorship contribution statement

Yeerang Lim: Writing – review & editing, Writing – original draft, Validation, Software, Methodology, Investigation, Data curation, Conceptualization. **Camilla Colombo:** Writing – review & editing,

Supervision, Project administration, Funding acquisition, Conceptualization.

Declaration of competing interest

The authors declare that they have no known competing financial interests or personal relationships that could have appeared to influence the work reported in this paper.

Acknowledgments

This research has received funding as part of the work developed for the agreement n. 2023-37-HH.0 for the project “Attività tecnico-scientifiche di supporto a C-SSA/ISOC e simulazione di architetture di sensori per SST”, established between ASI, Italian Space Agency, and POLIMI, Politecnico di Milano.

References

[1] R.P. Patera, Space event detection method, J. Spacecraft Rockets 45 (3) (2008) 554–559, https://doi.org/10.2514/1.30348.
[2] T. Kelecy, D. Hall, K. Hamada, D. Stocker, Satellite maneuver detection using two-line element (TLE) data, in: Proceedings of the Advanced Maui Optical and Space Surveillance Technologies Conference, Maui Economic Development Board (MEDB), Maui, HA, 2007, September, pp. 1–10.
[3] S. Lemmens, H. Krag, Two-line-elements-based maneuver detection methods for satellites in low earth orbit, J. Guid. Control Dynam. 37 (3) (2014) 860–868, https://doi.org/10.2514/1.61300.
[4] A. Pastor, G. Escribano, M. Sanjurjo-Rivo, D. Escobar, Satellite maneuver detection and estimation with optical survey observations, J. Astronaut. Sci. 69 (3) (2022) 879–917, https://doi.org/10.1007/s40295-022-00311-5.
[5] L. Porcelli, A. Pastor, A. Cano, G. Escribano, M. Sanjurjo-Rivo, D. Escobar, P. Di Lizia, Satellite maneuver detection and estimation with radar survey observations, Acta Astronaut. 201 (2022) 274–287, https://doi.org/10.1016/j.actaastro.2022.08.021.
[6] X. Zhou, D. Qiao, M. Macdonald, Orbit determination for impulsively maneuvering spacecraft using modified state transition tensor, J. Guid. Control Dynam. 47 (5) (2024) 822–839, https://doi.org/10.2514/1.G007814.
[7] H. Ren, X. Zhou, Q. Yang, Orbit determination of impulsively maneuvering spacecraft using adaptive state noise compensation, Symmetry 17 (4) (2025) 540, https://doi.org/10.3390/sym17040540.
[8] Y. Lim, C. Colombo, Manoeuvre identification and characterisation from two line elements, in: Proceedings of the 9th European Conference on Space Debris, ESA/ESOC, 2025, April, pp. 1–7.
[9] Crustal dynamics data information system (CDDIS), NASA, https://cddis.nasa.gov/archive/doris/products/orbits/ssa/.
[10] Space-track. https://www.space-track.org.
[11] R. Battin, An Introduction to the Mathematics and Methods of Astrodynamics, AIAA Education Series, AIAA, Reston, VA, 1999.
[12] L. Pirovano, R. Armellin, Detection and estimation of spacecraft maneuvers for catalog maintenance, Acta Astronaut. 215 (2024) 387–397, https://doi.org/10.1016/j.actaastro.2023.12.016.
[13] NASA general mission analysis tool (GMAT) version R2022a. https://software.nasa.gov/software/GSC-19097-1.
[14] A.W. Koenig, T. Guffanti, S. D'Amico, New state transition matrices for spacecraft relative motion in perturbed orbits, J. Guid. Control Dynam. 40 (7) (2017) 1749–1768.
[15] International laser ranging service (ILRS). https://ilrs.gsfc.nasa.gov/data_and_products/predictions/maneuver.html.
[16] A.A. Lidtke, D.J. Gondelach, R. Armellin, Optimising filtering of two-line element sets to increase re-entry prediction accuracy for GTO objects, Adv. Space Res. 63 (3) (2019) 1289–1317, https://doi.org/10.1016/j.asr.2018.10.018.